CrossMark

Stability-Guided Strategies to Mitigate Dendritic Growth in Lithium-Metal Batteries

Weiyu Li,[1] Hamdi A. Tchelepi,[1] Yiguang Ju,[2] and Daniel M. Tartakovsky[1,z] (ORCID)

[1]*Department of Energy Science and Engineering, Stanford University, Stanford, California 94305, United States of America*
[2]*Department of Mechanical and Aerospace Engineering, Princeton University, Princeton, NJ 08544, United States of America*

Dendritic growth is a leading cause of degradation and catastrophic failure of lithium-metal batteries. Deep understanding of this phenomenon would facilitate the design of strategies to reduce, or completely suppress, the instabilities characterizing electrodeposition on the lithium anode. We present a linear-stability analysis, which utilizes the Poisson-Nernst-Planck equations to describe Li-ion transport and, crucially, accounts for the lack of electroneutrality. This allows us to investigate the impact of electric-field gradients near the electrode surface on both ion diffusion and its anisotropy. Our analysis indicates that the use of anisotropic electrolytes (i.e., electrolytes with anisotropic diffusion coefficients of the Li ions) and the control of the local electric field can suppress dendritic growth of lithium metal. Specifically, changes in the local electric field can be used to enhance the longitudinal (perpendicular to the electrode) component of the cation diffusion coefficient tensor, which decreases the maximum growth rate of the dendrites. Electrolytes with electric field-dependent diffusion coefficients would reduce dendritic growth in small batteries, while anisotropic electrolytes (or separators with anisotropic pore structures or columnized membranes) are appropriate for batteries of any size.

Dendritic growth of lithium metal is a leading cause of degradation and catastrophic failure of Li-metal batteries. Understanding the unstable dendrite growth during electrodeposition, which has been observed in many experimental studies,[1–4] is crucial to the design and safe operation of Li-metal batteries. Linear stability analyses[5–9] can reveal important aspects of the dynamics associated with these instabilities. Of direct relevance to our study are investigations of the possible stabilizing effects of a negative background charge in porous media and of dependence of the crystal grain size on duty cycle in pulse electroplating.[10] Linear stability analyses of electrodeposition were also used to study the mechanical stabilization effects of external pressure,[11] elastic deformation[12] and electroconvection,[13] as well as other stabilization mechanisms such as thin-film piezoelectricity[14] and superimposition of AC forcing on a base DC field.[15]

These and other similar stability analyses rest on the assumption of local electroneutrality. Although this simplification is adequate under normal operating conditions, the deviation from electroneutrality can be significant when the applied current is high.[16] Investigations of this regime,[4,17,18] in which the cell overpotential ranged between 1.9 V and 3.7 V, aim to understand Li-metal battery cycling performance and dendrite growth on the fast-charging lithium-metal anode.[17] In such an overlimiting regime, the electrode surface becomes highly unstable.[19] The lack of electroneutrality implies the existence of an extended space-charge region[20] that significantly affects ion transport in the entire system.[21] It affects transport properties of the electrolyte, such as possible anisotropy of ion diffusion and dependence of the disparate diffusion coefficients of cations and anions on a strong electric field gradient near the electrode surface.

Anisotropy of ion diffusion in the electrolyte may provide a means to control dendritic growth of the lithium metal, because large gradients in the ion concentration parallel to the electrodes play a destabilizing role.[22] Dendrite formation and growth can be suppressed either by using an anisotropic electrolyte[23] or by inducing the anisotropy via application of an electric field, which engenders ionic drift diffusion and changes the transport properties.[24,25] Recent molecular dynamics simulations[26,27] also show that electric fields alter the diffusion coefficients of cations and anions in the electrolyte and render them direction-dependent.

Motivated by these findings, we perform a linear stability analysis of electrodeposition without resorting to the electroneutrality assumption. Our study extends the stability analysis[19] to include the mechanisms by which a local electric field close to the electrode surface alters ion diffusion and enhances its anisotropic behavior. The base- and perturbed-state Eqs. are solved numerically to compute the spatial distributions of the electric potential, charge density, and Li-ion concentration. These numerical solutions allow us to construct dispersion relations for the parameter space of interest. The comparison of the stability conditions with and without the electric field effects identifies potential mechanisms for reducing, and even suppressing, dendritic growth. In the vicinity of the electrode surface, larger values of the applied electric potential magnify the impact of (potential-dependent) ionic diffusivity on both the maximum growth rate and charge density. For example, the maximum growth rate is about 24% smaller than its counterpart for the constant isotropic diffusion coefficient.

Mathematical Formulation

We study electrodeposition on the lithium anode in a two-dimensional half-cell domain, $\Omega = \Omega_s \cup \Omega_f$ (Fig. 1). The Li-metal electrode surface $\Gamma(t)$, which separates the Li-metal anode $\Omega_s(t)$ from the liquid electrolyte $\Omega_f(t)$, is initially located at $x = 0$. A negative electrostatic potential, ϕ_e, is maintained on $\Gamma(t)$; the electric potential at the outer edge of the electrolyte $(x = L)$ is fixed at 0. The initial concentration of lithium cations, Li^+, in the binary dilute electrolyte is c_0. At the electrode surface, Γ, the cations, Li^+, undergo a Faradaic reaction with electrons, e^-, and reduce to Li atoms, $Li^+ + e^- \rightarrow Li$, which are subsequently deposited on the electrode surface.

This deposition causes the Li-metal surface $\Gamma(t)$ to change with time t. We study this evolution in the two-dimensional Cartesian coordinate system spanned by the orthogonal unit-vectors $\mathbf{e}_x$ and $\mathbf{e}_y$, and represent the moving interface, $\Gamma(t)$, by a single-valued function $h(y, t)$ such that $h(y, 0) = 0$ (Fig. 1). Our focus is on the stability of the electrodeposition, i.e., of the temporal evolution of $h(y, t)$.

Governing equations.—Under isothermal conditions and in the absence of a magnetic field, the state of an immobile dilute electrolyte at any point $\mathbf{x} = (x, y)^\top \in \Omega_f = \{\mathbf{x}: h(y, t) \leqslant x \leqslant L, 0 \leqslant y \leqslant B\}$ and time t is defined by the concentrations (mol/m^3) of cations, $c_+(\mathbf{x}, t)$, and anions, $c_-(\mathbf{x}, t)$, and by the electric potential $\phi(\mathbf{x}, t)$ (V). Spatial variability of these three state variables induces
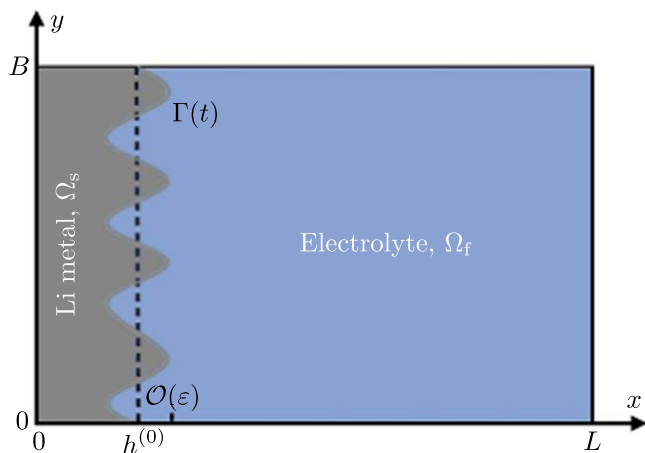
Figure 1. Schematic representation of a two-dimensional half-cell domain $\Omega = \Omega_s \cup \Omega_f$. The interface between the Li metal, Ω_s, and liquid electrolyte, Ω_f, is denoted by Γ. The coordinate system moves in the positive x direction with velocity U, which is the average deposition rate on the electrode.

mass fluxes of cations, $\mathbf{J}_+(\mathbf{x}, t)$, and anions, $\mathbf{J}_-(\mathbf{x}, t)$,

$$\mathbf{J}_\pm = -\mathbf{D}_\pm\left(\nabla c_\pm + \frac{z_\pm c_\pm F}{RT}\nabla\phi\right), \qquad [1a]$$

where $\mathbf{D}_\pm$ are the diffusion coefficients ($m^2\,s^{-1}$), whose tensorial nature accounts for possible anisotropy; $z_\pm$ are the charge numbers (valences) of the cations and anions; F is the Faraday constant ($s\cdot A\,mol^{-1}$); R is the gas constant (J/mol/K); and T is the temperature (K). Mass conservation of ions in the electrolyte is described by the Nernst-Planck equations,

$$\frac{\partial c_\pm}{\partial t} = -\nabla\cdot\mathbf{J}_\pm, \qquad \mathbf{x}\in\Omega_f, \quad t > 0. \qquad [1b]$$

The electric potential, ϕ, is governed by the Poisson equation,

$$-\epsilon\nabla^2\phi = z_+ F c_+ + z_- F c_-, \qquad \mathbf{x}\in\Omega_f, \quad t > 0, \qquad [2]$$

where ϵ is the absolute permittivity of the solvent ($F\,m^{-1}$).

The electrode's surface $\Gamma(t)$ is impervious to inert (non-reactive) anions, i.e.,

$$\mathbf{n}\cdot\mathbf{J}_- = 0, \qquad \mathbf{x}\in\Gamma, \quad t > 0, \qquad [3]$$

where $\mathbf{n}$ is the normal vector pointing outward from the electrolyte. The normal component of the cation flux, $\mathbf{J}_+$, through this surface is balanced by the Faradaic reaction $Li^+ + e^- \rightarrow Li$ such that

$$\mathbf{n}\cdot\mathbf{J}_+ = R_{Li}, \qquad \mathbf{x}\in\Gamma, \quad t > 0, \qquad [4a]$$

where R_{Li} is the rate of production of lithium atoms.[10] This condition is supplemented with the minimum Li^+ concentration condition at the electrode surface:[19]

$$\mathbf{n}\cdot\nabla c_+ = 0, \qquad \mathbf{x}\in\Gamma, \quad t > 0. \qquad [4b]$$

The production rate R_{Li} is given by the Butler-Volmer equation,

$$R_{Li} = -\frac{k_0}{\gamma_{ts}}\left[\exp\left(\alpha_{an}\frac{zF\eta_\alpha + 2\omega\gamma\kappa}{RT}\right) - \frac{c_+(\mathbf{x}\in\Gamma, t)}{c_+^\Theta}\exp\left(-\alpha_{cat}\frac{zF\eta_\alpha + 2\omega\gamma\kappa}{RT}\right)\right], \qquad [5]$$

where k_0 is the reaction rate constant ($mol/m^2\,s^{-1}$); γ_{ts} is the activity coefficient of the transition state for the Faradaic reaction $(-)$; z is the number of electrons involved in the electrode reaction; and α_{an} and

α_{cat} are the anodic and cathodic charge-transfer coefficients, respectively $(-)$; c_+^Θ is the standard concentration; ω is the molar volume of Li metal ($m^3\,mol^{-1}$); γ is the isotropic surface energy of the Li metal ($J\,m^{-2}$), and $\kappa(y, t)$ is the mean curvature of $\Gamma(t)$ (m^{-1}). The activation overpotential $\eta_\alpha(\mathbf{x}\in\Gamma, t)$ is defined as

$$\eta_\alpha = \phi_e - \phi(\mathbf{x}\in\Gamma, t) - E^\Theta, \qquad [6]$$

where E^Θ is the standard electrode potential. For the sake of specificity, we set $\gamma_{ts} = 1$, $\alpha_{an} = 1 - \alpha_{cat}$, and $E^\Theta = 0$. The interfacial current density I is related to the reaction rate R_{Li} by

$$I = zFR_{Li}. \qquad [7]$$

The boundary conditions on the moving interface $\Gamma(t)$, Eqs. 3 and 4, are supplemented with a kinematic condition that describes the spatiotemporal evolution of Γ. The normal-vector $\mathbf{n}(y, t)$ and mean curvature $\kappa(y, t)$ of Γ are expressed in terms of the derivatives of $h(y, t)$ as[19]

$$\mathbf{n} = \frac{1}{\sqrt{1 + (\partial_y h)^2}}\begin{pmatrix} -1 \\ \partial_y h \end{pmatrix},$$

$$\kappa = -\frac{1}{2}\frac{\partial_y^2 h}{[1 + (\partial_y h)^2]^{3/2}}. \qquad [8]$$

The rate of change of $\Gamma(t)$, or equivalently of $h(y, t)$, is given by the current into the anode,[10,19]

$$\mathbf{e}_x\cdot\mathbf{n}\frac{\partial h(y, t)}{\partial t} = -\frac{\omega I}{zF}. \qquad [9]$$

The boundary conditions on the remaining segments of the computational domain Ω_f are

$$\phi = 0, \qquad c_+ = c_0, \qquad c_- = c_0, \qquad \text{for } x = L; \qquad [10a]$$

$$\frac{\partial\phi}{\partial y} = 0, \qquad \frac{\partial c_+}{\partial y} = 0, \qquad \frac{\partial c_-}{\partial y} = 0, \qquad \text{for } y = 0 \text{ and } B. \qquad [10b]$$

The boundary conditions at $x = L$ reflect an assumption that small (magnitude ε) perturbations of the anode surface do not affect the ion concentrations the half-cell distance away; this assumption is effectively enforced in the full-cell linear stability analyses[10,19] that impose identical perturbations on both cathode and anode (Fig. 8 provides a comparison of our results with those reported in 10). The last three boundary conditions in Eq. 10 imply that the horizontal surfaces, $y = 0$ and B, are electrically insulated and impermeable.

Diffusivity alteration by electric field.—The presence of an electric field, $\mathbf{E} = (E_x = -\partial_x\phi, E_y = -\partial_y\phi)^\top$, alters the diffusion coefficients of cations and anions, $D_\pm$, rendering them direction-dependent, $\mathbf{D}_\pm$.[26,27] Both the magnitude of the diffusion coefficients and the degree of their anisotropy increase with the magnitude of E_x or E_y. We adopt the exponential model derived from the molecular dynamics simulations of 1M solution of LiPF$_6$ in ethylene carbonate,[26]

$$\mathbf{D}_\pm = D_\pm^{\text{ref}}\begin{pmatrix} e^{b_\pm|E_x|} & 0 \\ 0 & e^{b_\pm|E_y|} \end{pmatrix}$$

$$= D_\pm^{\text{ref}}\begin{pmatrix} e^{b_\pm\partial_x\phi} & 0 \\ 0 & e^{b_\pm\partial_y\phi} \end{pmatrix}. \qquad [11]$$

where $D_\pm^{\text{ref}}$ are the isotropic diffusion coefficients of cations and anions when $|\mathbf{E}| = 0$, and the fitting parameters $b_\pm$ ($m\,V^{-1}$) account for the strength of the electric field.

Like many others, our model of dendritic growth, Eqs. 1–10, rests on the dilute-solution formulation. Measurements of the activity coefficient for LiPF$_6$ in PC/EC/DMC for a wide range of concentration (up to 4M) found it to be close to 1 for concentrations up to 1M,[28] indicating that the dilute formulation holds. This finding is seemingly contradicted by the study[29] that found the solutions of LiPF$_6$ in PC/EC/EMC for the concentration range 0.0625–1M not to be "dilute"; yet, it showed that the dilute-solution model of these solutions overestimates the specific energy of a lithium-ion cell by only 0.6%. Be that as it may, our analysis can accommodate other dependencies of $\mathbf{D}_\pm$ on $\mathbf{E}$, and the one in Eq. 11 is used for the sake of concreteness.

Linear Stability Analysis

Linear stability analysis is performed by applying a small perturbation, $\varepsilon \exp(wt + iky)$, to a one-dimensional steady-state base state, $h^{(0)}(t) \equiv Ut$, $\phi^{(0)}(x)$ and $c_\pm^{(0)}(x)$. Here, ε is the small dimensionless parameter, w is the growth rate (1/s), k is the wave number (1/m), and $i^2 = -1$. The electrodeposition process is unstable if the perturbations grow with time, i.e., if $w > 0$. The goal of a stability analysis is to express w in terms of the physical properties of the electrolyte and the anode.

To facilitate this analysis, we rewrite 1–11 in terms of dimensionless variables

$$\tilde{x} = \frac{x}{L}, \quad \tilde{y} = \frac{y}{L}, \quad \tilde{t} = \frac{tD_+^{\text{ref}}}{L^2}, \quad \tilde{c}_\pm = \frac{c_\pm}{c_0},$$

$$\tilde{\phi} = \frac{F\phi}{RT}, \quad \tilde{h} = \frac{h}{L}, \quad \tilde{U} = \frac{UL}{D_+^{\text{ref}}},$$

$$\tilde{D}_\pm = \frac{D_\pm}{D_+^{\text{ref}}}, \quad \tilde{b}_\pm = \frac{RTb_\pm}{FL}, \quad \tilde{\lambda}_D^2 = \frac{RT\epsilon}{2L^2F^2c_0},$$

$$Ca = \frac{\omega\gamma}{RTL}, \quad \tilde{R}_{Li} = \frac{LR_{Li}}{D_+^{\text{ref}}c_0}. \qquad [12a]$$

The corresponding dimensionless parameters describing the perturbation of the anode surface, Γ, are

$$\tilde{k} = kL, \qquad \tilde{w} = \frac{L^2w}{D_+^{\text{ref}}}. \qquad [12b]$$

The dimensionless Li production rate $\tilde{R}_{Li}$ and interfacial current density $\tilde{I}$ are

$$\tilde{R}_{Li} = -\tilde{k}_0 e^{-\alpha_{cat}(z\tilde{\eta}_\alpha + 2\tilde{\omega}\tilde{\kappa})} \left[e^{z\tilde{\eta}_\alpha + 2Ca\tilde{\kappa}} - \frac{\tilde{c}_+}{\tilde{c}_+^\Theta} \right],$$

$$\tilde{I} = \frac{I}{I_{lim}} = \frac{z\tilde{R}_{Li}}{2}, \qquad [12c]$$

where

$$\tilde{k}_0 = \frac{Lk_0}{D_+^{\text{ref}}c_0\gamma_{ts}}, \quad \tilde{\eta}_\alpha = \frac{F\eta_\alpha}{RT}, \quad \tilde{\kappa} = L\kappa,$$

$$\tilde{c}_+^\Theta = \frac{\tilde{c}_+^\Theta}{c_0}, \quad I_{lim} = \frac{2FD_+^{\text{ref}}c_0}{L}. \qquad [12d]$$

Unless specified otherwise, all the quantities discussed from here on are dimensionless, even though we drop the tildes to simplify the notation. In a linear analysis, the electrode surface height, $h(y, t)$, and the state variables $\phi(x, y, t)$ and $c_\pm(\mathbf{x}, t)$ are written as

$$h(y, t) = h^{(0)}(t) + \varepsilon h^{(1)} e^{wt+iky} \qquad [13]$$

$$\phi(\mathbf{x}, t) = \phi^{(0)}(x) + \varepsilon\phi^{(1)}(x)e^{wt+iky} \qquad [14]$$
$$c_\pm(\mathbf{x}, t) = c_\pm^{(0)}(x) + \varepsilon c_\pm^{(1)}(x)e^{wt+iky}, \qquad [15]$$

where the constant $h^{(1)}$ and the functions $\phi^{(1)}$ and $c_\pm^{(1)}$ are the first-order (in ε) corrections. Then, the interfacial conditions 3–11 are expanded in Taylor series around the leading-order interface $h^{(0)}$, which is moving with the constant velocity $U = dh^{(0)}/dt = -\omega R_{Li}^{(0)}$; e.g., $\phi(\mathbf{x} \in \Gamma, t) \approx \phi(h^{(0)}, y, t) + \dots$. Finally, the terms of equal power of ε are collected to specify boundary-value problems (BVPs) for the base state (of order ε^0) and the first-order correction (of order ε). These calculations are reported in the Appendix; the BVP for the base-state variables $c_\pm^{(0)}(\xi)$ and $\phi^{(0)}(\xi)$ consists of Eqs. 23a and 24, and the BVP for the perturbed-state variables $c_\pm^{(1)}(\xi)$ and $\phi^{(1)}(\xi)$ comprises Eqs. 25 and 26. Both BVPs are written in the moving coordinate system ($\xi \equiv x + \omega R_{Li}^{(0)}t, y)^\top$.

The base-state Eqs. 23a and 24 are solved numerically with the Matlab function `bvp4c` to obtain $c_\pm^{(0)}(\xi)$, $\phi^{(0)}(\xi)$, and their first- and second-order derivatives. These are then used as coefficients in the perturbed-state Eqs. 25 and 26; the numerical solution is obtained[10] by employing a second-order finite-difference scheme and solving the resulting generalized eigenvalue problem with the Matlab function `eigs`.

Table I. Parameters used in the simulations.

Parameter	Symbol	Value	Units	References
Half-cell length	L	0.5, 5, 50	μm	19
Cation diffusivity without electric field	D_+^{ref}	$1.61 \cdot 10^{-11}$	m^2 s^{-1}	30
Anion diffusivity without electric field	D_-^{ref}	$3.91 \cdot 10^{-11}$	m^2 s^{-1}	30
Exponent in cation diffusion tensor	b_+	$2.31 \cdot 10^{-9}$	m V^{-1}	26
Exponent in anion diffusion tensor	b_-	$2.49 \cdot 10^{-9}$	m V^{-1}	26
Temperature	T	298.15	K	
Molecular weight of lithium metal	M	6.941	g mol^{-1}	31
Density of lithium metal	ρ	0.534	g cm^{-3}	31
Li$^+$ bulk concentration	c_0	1000	mol/m^3	
Standard concentration	c_{ref}	1000	mol m^{-3}	
Standard electrode potential	E^Θ	0	V	
Dielectric constant	ϵ/ϵ_0	90	—	32
Vacuum permittivity	ϵ_0	$8.854 \cdot 10^{-12}$	F m^{-1}	33
Reaction rate constant	k_0	$2.7 \cdot 10^{-3}$	mol (m$^2 \cdot$ s)$^{-1}$	34
Surface energy of metal/electrolyte interface	γ	1	J m^{-2}	7
Activity coefficient of the transition state	γ_{ts}	1	—	
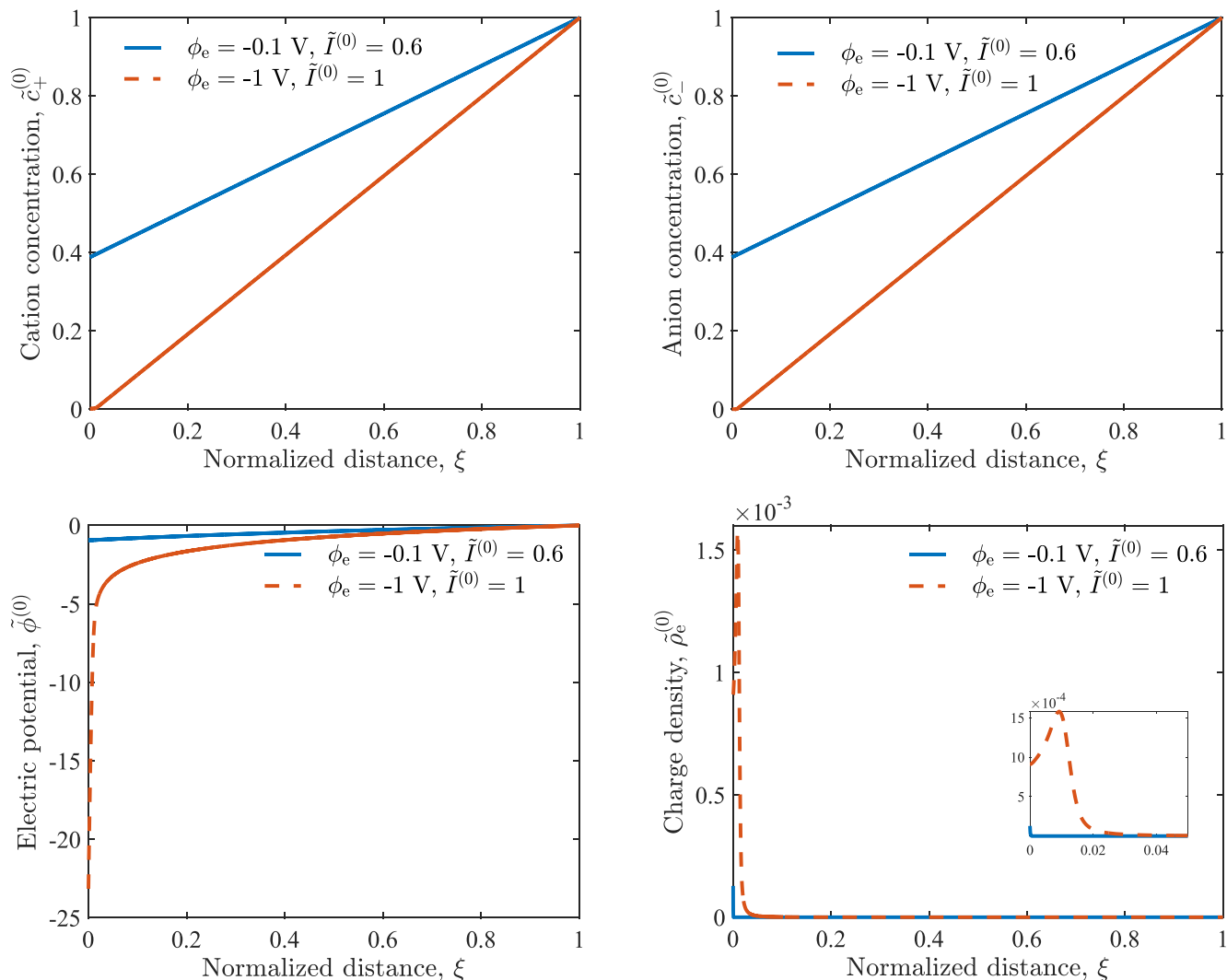
Figure 2. Spatial profiles of the base-state cation, $\tilde{c}_+^{(0)}$, and anion, $\tilde{c}_-^{(0)}$, concentrations; electric potential $\tilde{\phi}^{(0)}$; and charge density $\tilde{\rho}_e^{(0)}$ for $L = 5\ \mu$m, $\phi_e = -0.1$ V or -1 V, and constant diffusion coefficients $D_\pm = D_\pm^{\text{ref}}$.

Results and Discussion

The parameters used in our simulations are presented in Table I. We start by computing the base-state solution for constant isotropic diffusion coefficients, $D_\pm$, (i.e., for Eq. 11 with $b_\pm = 0$) for a wide range of the applied electric potential ϕ_e. Figure 2 shows the concentrations of cations, $\tilde{c}_+^{(0)}$, and anions, $\tilde{c}_-^{(0)}$; the charge density $\tilde{\rho}_e^{(0)} = \tilde{c}_+^{(0)} - \tilde{c}_-^{(0)}$; and the electric potential $\tilde{\phi}^{(0)}$. These dimensionless quantities are computed for the half-cell length $L = 5\ \mu$m, which corresponds to the limiting current density $I_{lim} = 2FD_+^{\text{ref}} c_0 / L = 62.1$ mA/cm². For small values of the applied potential, $\phi_e = -0.1$ V, the base-state current density $I^{(0)}$ is smaller than I_{lim}, the cations at the electrode surface are not depleted, and electroneutrality holds throughout the simulation domain. On the other hand, for large ϕ_e when $I^{(0)}$ reaches I_{lim}, the Li-cation concentration $c_+^{(0)}(\xi)$ is approximately zero near the electrode surface and local electroneutrality is violated within the boundary layer, $0 \leqslant \tilde{\xi} \leqslant 0.02$; for $L = 5\ \mu$m, its width is $0.02 \cdot 5 = 0.1\ \mu$m. Figure 2 also shows that higher values of the applied potential ϕ_e induce larger values of the electric potential gradient, $\partial_\xi \phi^{(0)}$, near the electrode surface.

In accordance with Eq. 11, the electric field $\mathbf{E} = -\nabla\phi$ gives rise to anisotropic ionic diffusion. Since for the base state $\mathbf{E}^{(0)} = (-j_\phi^{(0)}, 0)^\top$, the leading-order approximations of the principal components of the diffusion tensor $\mathbf{D}_\pm^{(0)}$ in Eq. 17 become

$D_{xx}^\pm = D_\pm^{\text{ref}} \exp(b_\pm j_\phi^{(0)})$ and $D_{yy}^\pm = D_\pm^{\text{ref}}$, i.e., the diffusion anisotropy manifests itself in the boundary layer adjacent to the electrode. Figure 3 shows the spatial extent of this region for half-cell lengths $L = 0.5$ and $5\ \mu$m. Both the anisotropy ratio D_{xx}^+/D_{yy}^+ and the boundary-layer width increase as L decreases, or ϕ_e increases, with the longitudinal diffusion coefficient D_{xx}^+ being up to 12% larger than its reference value D_+^{ref} for $L = 0.5\ \mu$m and $\phi_e = -3.5$ V.

Next, we investigate the impact of the electric field-dependence of ion diffusion on electrodeposition. Specifically, we compare the base-state charge density $\tilde{\rho}_e^{(0)}$ and the perturbed-state growth rates $\tilde{w}$ alternatively computed with either constant diffusion coefficients $D_\pm^{\text{ref}}$ or field-dependent diffusion coefficients $\mathbf{D}_\pm$ in Eq. 17. When the applied electric potential is small ($\phi_e = -0.1$ V) the dependence of the diffusion coefficients on the electric field has negligible effect on the charge density $\tilde{\rho}_e$ (Fig. 4). This is because in this regime the electric field E is approximately zero (Fig. 2). Higher values of the applied electric potential ($\phi_e = -2.5$ and -3.5 V) produce the boundary layer within which the electrolyte is not electroneutral, $E > 0$, the diffusion anisotropy increases in accordance with Eq. 17, and the base-state charge density $\tilde{\rho}_e^{(0)}$ near the electrode surface decreases relative to that predicted for the constant diffusion coefficient.
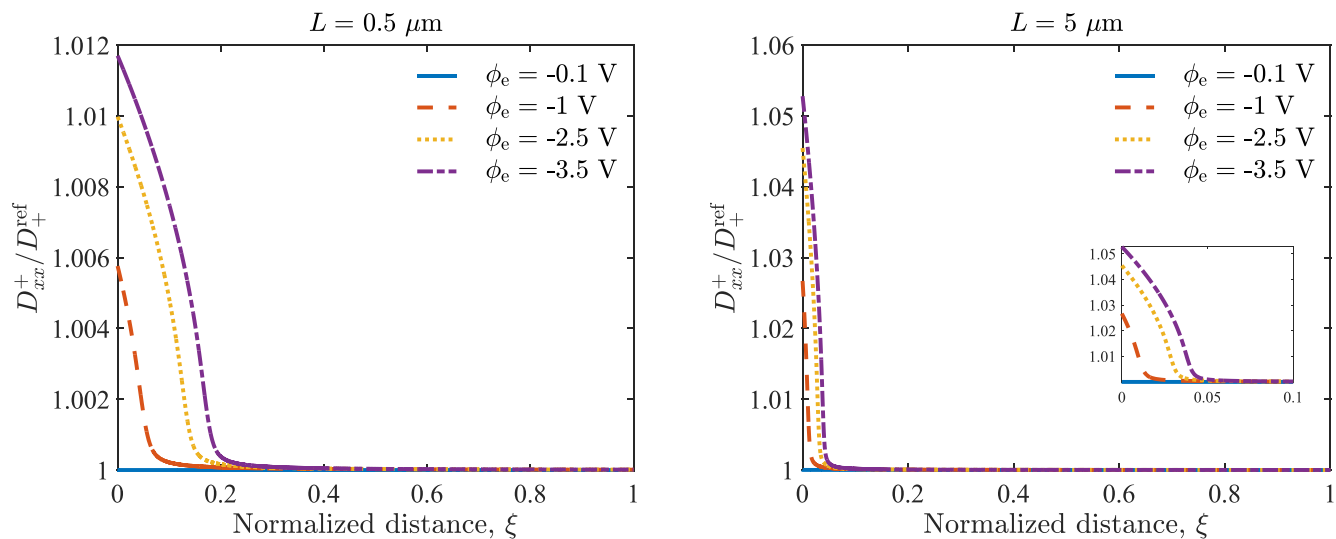
Figure 3. Spatial profiles of the normalized longitudinal diffusion coefficient, $D_{xx}^+/D_+^{\text{ref}}$ in Eq. 17, for $L = 0.5$ and 5 μm and several values of ϕ_e.
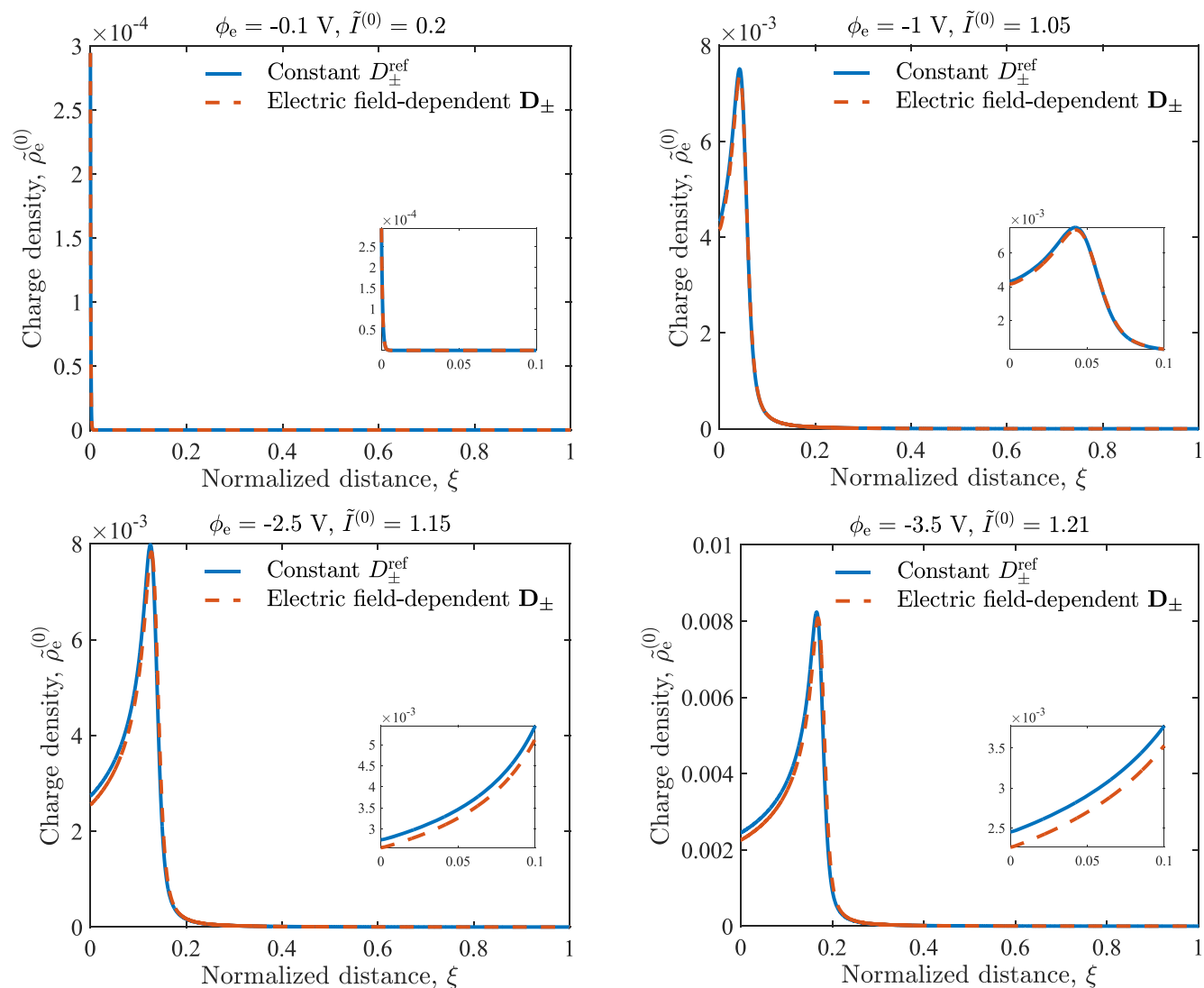
Figure 4. Spatial profiles of base-state charge density $\tilde{\rho}_e^{(0)}$ computed with either constant diffusion coefficients $D_\pm^{\text{ref}}$ or electric field-dependent diffusion coefficients $\mathbf{D}_\pm$ in Eq. 17, for $L = 0.5$ μm and several values of ϕ_e.

Figure 5. Dispersion relations $\tilde{w} = \tilde{w}(\tilde{k})$ computed with either constant diffusion coefficients $D_\pm^{\text{ref}}$ or electric field-dependent diffusion coefficients $\mathbf{D}_\pm$ in Eq. 17, for $L = 0.5 \ \mu$m and several values of ϕ_e.

These relatively small and localized changes in electroneutrality (Fig. 2) and charge density (Fig. 4) have significant impacts on the dendrite growth rate $\tilde{w}$ when the applied electric potential ϕ_e becomes large (Fig. 5). For small ϕ_e, i.e., for underlimiting current ($I^{(0)} < I_{lim}$), the growth rate $\tilde{w}$ is negative for all wavenumbers $\tilde{k} > 0$. This means that the electrode surface growth is unconditionally stable, i.e., a small initial perturbation of the surface geometry decays with time, regardless of whether or not the diffusion tensor $\mathbf{D}_\pm$ depends on the electric field $\mathbf{E}$. For larger ϕ_e (overlimiting current, $I^{(0)} > I_{lim}$), the growth rate $\tilde{w}$ is positive within a certain range of $\tilde{k}$, where the surface growth is unstable and dendrites develop. The dispersion relation $\tilde{w} = \tilde{w}(\tilde{k})$ exhibits non-monotonic behavior: $\tilde{w}$ increases from zero at $\tilde{k} = 0$ to its maximum value of $\tilde{w}_{max}$ at $\tilde{k}_{max}$ wherein the electrode surface growth is maximally unstable; further increase of $\tilde{k}$ causes the positive growth rate $\tilde{w}$ to decrease until it reaches 0 at a critical wavenumber $\tilde{k}_{cr}$ at which point the electrode surface is marginally stable. For $\tilde{k} > \tilde{k}_{cr}$, the growth rate $\tilde{w}$ becomes negative, and surface energy stabilizes the electrode surface growth. The surface energy term $Ca \ \tilde{k}^2$ in Eqs. 25–26 comprises the surface curvature $\kappa^{(1)} \propto k^2$ and the surface energy γ. This term has a stabilizing effect on the surface growth at

large $\tilde{k}$ by imposing an energy penalty on the creation of additional surface area. The difference between the dispersion relations $\tilde{w} = \tilde{w}(\tilde{k})$ corresponding to constant diffusion coefficients $D_\pm^{\text{ref}}$ and their electric field-dependent anisotropic counterparts $\mathbf{D}_\pm$ increases with ϕ_e. For $\phi_e = -3.5$ V, the use of $D_\pm^{\text{ref}}$ instead of $\mathbf{D}_\pm$ would overestimate $\tilde{w}_{max}$ by 24%, while k_{cr} remains virtually unchanged.

In another set of numerical experiments, we study how the half-cell length L affects the stability of the electrode interface growth. Figure 6 shows the dispersion relations $\tilde{w} = \tilde{w}(\tilde{k})$ corresponding to constant isotropic diffusion coefficients $D_\pm^{\text{ref}}$ and the electric field-dependent diffusion tensors $\mathbf{D}_\pm$, for $L = 5 \ \mu$m (although not shown here, we have observed the same trend for $L = 50 \ \mu$m). The maximum growth rate $\tilde{w}_{max}$ increases with L, which is in agreement with the previous study.[19] The impact of the electric field-dependency of the diffusion coefficient on the dispersion relation $\tilde{w} = \tilde{w}(\tilde{k})$ decreases with L. That is because the change in $\tilde{D}_{xx}^\pm$ is confined to the boundary layer adjacent to the electrode, and the width of this layer as a small fraction of the total cell decreases with L (Fig. 3).

The local electric field impacts ion diffusion in two ways: it alters the magnitude of the ionic diffusion coefficients and enhances their
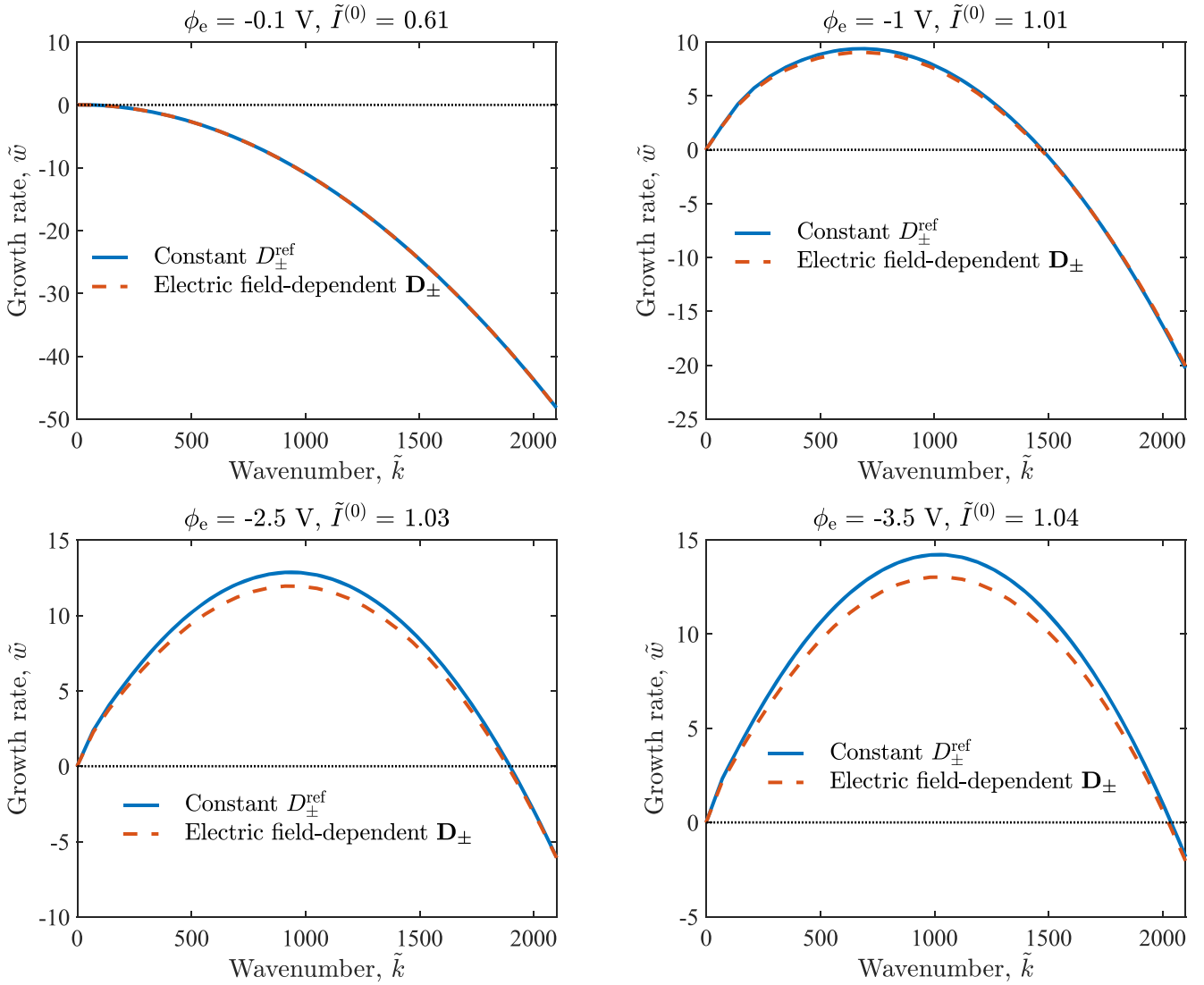
Figure 6. Dispersion relations $\tilde{w} = \tilde{w}(\tilde{k})$ computed with either constant diffusion coefficients $D_{\pm}^{\text{ref}}$ or electric field-dependent diffusion coefficients $\mathbf{D}_{\pm}$ in Eq. 17, for $L = 5$ μm and several values of ϕ_e.
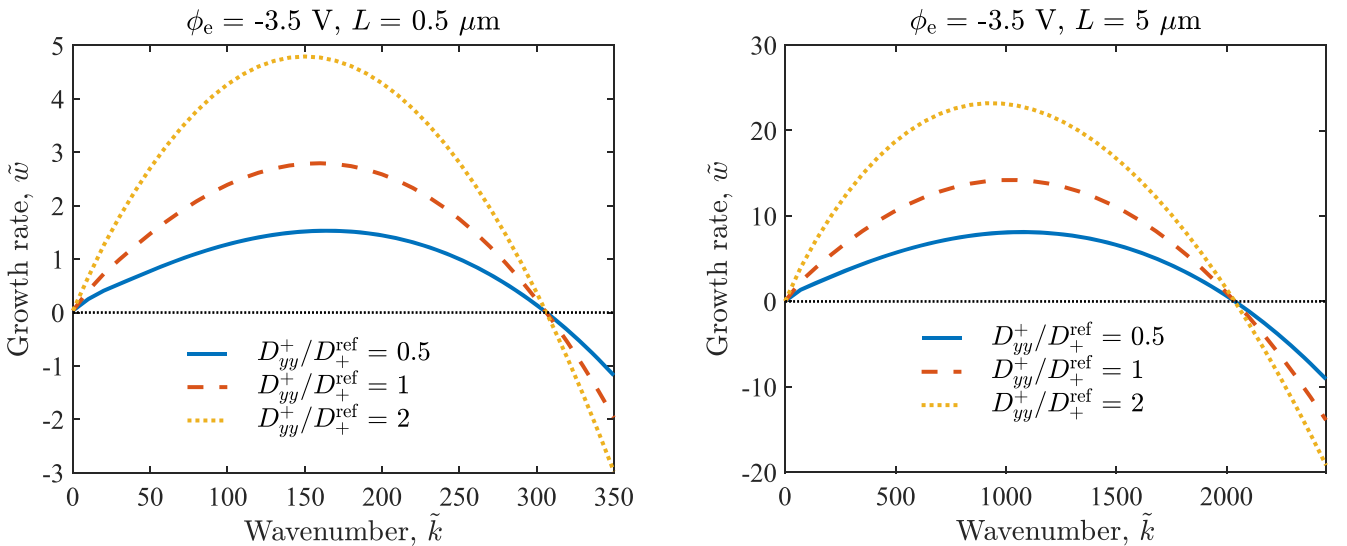
Figure 7. Dispersion relations $\tilde{w} = \tilde{w}(\tilde{k})$ computed with either constant isotropic diffusion coefficients $D_{\pm}^{\text{ref}}$ or constant anisotropic diffusion coefficients $D_{xx}^+ = D_+^{\text{ref}}$, $D_{yy}^- = D_{xx}^- = D_-^{\text{ref}}$ and two values of D_{yy}^+. Other parameters are set to $\phi_e = -3.5$ V and to either $L = 0.5$ μm or $L = 5$ μm.
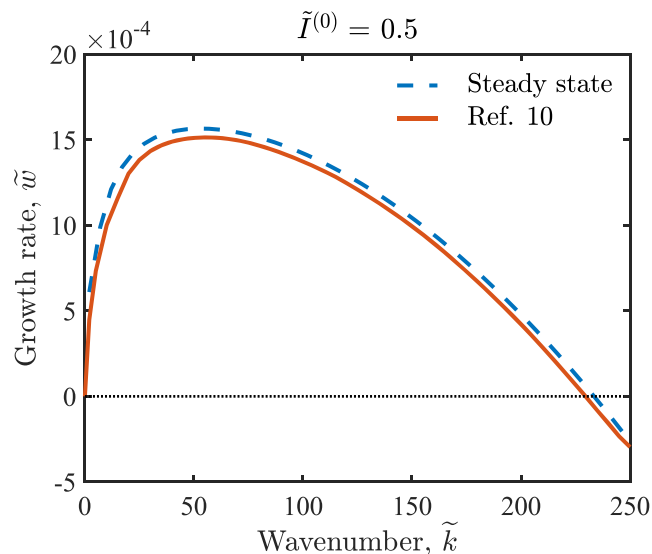
Figure 8. Dispersion relations $\tilde{w} = \tilde{w}(\tilde{k})$ alternatively predicted with the steady-state and transient base-state solutions. The latter is obtained by extracting the data from Fig. 2 in the Supplementary Material for 10.

anisotropic nature. To isolate the contribution of each factor, we conduct two sets of numerical experiments. In the first, we simulate electrolytes with isotropic diffusion coefficients $D_\pm = D_\pm^{\text{ref}}$; with $D_\pm = 1000 D_\pm^{\text{ref}}$; and with the anion diffusivity $D_- = D_-^{\text{ref}}$ and the cation diffusivity $D_+ = 1000 D_+^{\text{ref}}$. Although not shown here, we found that modifying D_- has no effect and modifying D_+ has a negligible effect on the dispersion relations in Fig. 5 and 6.

The second set of experiments deals with the stability analysis for electrolytes with constant anisotropic diffusion coefficients,

$$\mathbf{D}_\pm = \begin{pmatrix} D_{xx}^\pm & 0 \\ 0 & D_{yy}^\pm \end{pmatrix}. \qquad [16]$$

where $D_{xx}^\pm$ and $D_{yy}^\pm$ are the constant diffusion coefficient components in the principal x and y directions. The resulting base-state and perturbed-state Eqs. are derived in the Appendix. We found the anisotropic behavior of the anion diffusion coefficient $\mathbf{D}_-$ to have no impact on the interfacial dynamics, so we only present results for different anisotropy ratios of the cation diffusion coefficient $\mathbf{D}_+$. The use of $\mathbf{D}_\pm$ from Eq. 16 rather than from Eq. 11 does not change the base-state dynamics, which is governed by Eqs. 23a and 24. The perturbed-state Eqs. are reported in the Appendix. Figure 7 exhibits the dispersion relations $\tilde{w} = \tilde{w}(\tilde{k})$ corresponding to the constant isotropic diffusion coefficients $D_\pm^{\text{ref}}$ and to the constant anisotropic diffusion coefficients $D_{xx}^+ = D_+^{\text{ref}}$, $D_{yy}^- = D_{xx}^- = D_-^{\text{ref}}$ and two values of D_{yy}^+. The maximum growth rate $\tilde{w}_{max}$ increases by about 70% or 60% when D_{yy}^+ doubles from D_+^{ref} to $2D_+^{\text{ref}}$, for $\phi_e = -3.5$ V and $L = 0.5$ μm or $L = 5$ μm, respectively. Enhancing cation diffusion in the direction parallel to the electrode surface (y) decreases the maximum wavenumber $\tilde{k}_{max}$, while the critical wavenumber $\tilde{k}_c$ remains unchanged. This finding is in agreement with the numerical simulations of dendrite growth.[23] It is worthwhile contrasting this behavior with that of interfacial growth in multiphase flows,[35–38] in which increasing the transverse component of the diffusion coefficient tensor stabilizes the interface.

Our stability analysis follows the large body of literature[7,9,13,19,39,40] in assuming the base state to be stationary. The transient base-state analysis[10] reveals this assumption to have no effect on the dispersion relation $w = w(k)$ when the current density I is much smaller than the

limiting current I_{lim} (Fig. 8). The importance of the transient base state becomes more pronounced in the over-limiting regime, $I > I_{lim}$, (see Fig. 5 in [10]). However, in this regime the electroneutrality assumption, which underpins the stability analysis in [10], no longer holds. In a follow-up study, we will extend our analysis to account for the transient base state.

Conclusions

To identify possible mechanisms for control of dendrite growth in Li-metal batteries, we conducted a linear stability analysis of electrodeposition onto the electrode surface. The analysis employs the Poisson-Nernst-Planck Eqs. coupled with the Butler-Volmer kinetics to describe electrodeposition. we do not invoke the assumption of electroneutrality, which is known to break down in the boundary layer adjacent to the electrode surface. Accounting for gradients in the charge distributions allowed us to investigate the stabilizing effects of electric field-dependent anisotropic diffusion of ions on dendritic growth of Li. Our analysis leads to the following major conclusions.

• Electric field-dependent anisotropic diffusion reduces both charge density close to the electrode surface and the maximum growth rate of dendrites relative to the values of their counterparts for constant isotropic diffusion.
• This effect is most pronounced for large values of the applied electric potential ϕ_e and small half-cell lengths L, e.g., the maximum growth rate is reduced by about 24% when $\phi_e = -3.5$ V and $L = 0.5$ μm. Hence, the impact of electric field on ionic diffusion cannot be ignored for batteries with ultra-thin separators.
• The local electric field affects ion diffusion and the stability of electrodeposition by altering the diffusion coefficient values and by enhancing the degree of anisotropy. An interplay of these two mechanisms can be used to suppress dendritic growth in Li-ion and Li-metal batteries.

Our findings suggest new strategies for the electrolyte design, i.e., for the optimal selection of solvent and salt and for the tuning of the ionic concentration of solution. Such a design would be informed by the degree to which the electric field affects the electrolyte's transport properties and anisotropic behavior and, ultimately, the dendritic growth. An optimal electrolyte (with additives) would exhibit a strong response to the local electric field in a way that increases the cation diffusion coefficient in the direction perpendicular to the electrode surface.

Another design strategy for the suppression of dendrite growth, suggested by our analysis, is to use anisotropic electrolytes, e.g., liquid crystals, liquid-crystalline physical gels etc., or separators with anisotropic pore structures or columnized membranes. As a dendrite suppression strategy, electrolytes with electric field-dependent diffusion coefficients are appropriate for small batteries, while anisotropic electrolytes reduce dendritic growth in batteries of any size.

Although our linear stability analysis reveals the role of key parameters in dendrite initiation, it does not describe subsequent dendritic growth. The latter requires a numerical solution of surface-evolution equations. In follow-up studies, we will model the dynamics of dendritic growth by solving the nonlinear phase-field equations[41,42] and compare this solution with the predictions of our linear stability analysis. We also plan to compare the advantages and disadvantages of commonly used commercial liquid electrolytes[43] and to investigate the effects of coating on the dendritic growth of the solid electrolyte surface. The former study would require electrolyte-specific experimental data on the dependence of ionic diffusion coefficients on applied electric field, while the latter analysis will be facilitated by an effective-medium representation[44] of the composite solid electrolyte.

Finally, it is worthwhile emphasizing that our analysis ignores several interfacial phenomena on the anode, which are of potential relevance to Li-dendrite initiation and growth. These include

Li-solvation/desolvation and their impact on the formation of solid electrolyte interface.[45,46] Accounting for these processes is another fruitful venue for future research.

Appendix A. Perturbation Analysis

Let $\hat{\varepsilon} = \varepsilon \exp(wt + iky)$. Then, accounting for Eq. 14, a Taylor expansion of $\mathbf{D}_\pm$ in Eq. 11 is

$$\mathbf{D}_\pm = D_\pm^{\mathrm{ref}} \begin{pmatrix} e^{b_\pm j_\phi^{(0)}} & 0 \\ 0 & 1 \end{pmatrix}$$
$$+ \hat{\varepsilon} D_\pm^{\mathrm{ref}} b_\pm \begin{pmatrix} e^{b_\pm j_\phi^{(0)}} \partial_x \phi^{(1)} & 0 \\ 0 & ik\phi^{(1)} \end{pmatrix}$$
$$+ \mathcal{O}(\varepsilon^2)\mathbf{I}, \qquad [17]$$

where $j_\phi^{(0)} = \partial_x \phi^{(0)}$, and $\mathbf{I}$ is the 2×2 identity matrix. Substituting Eqs. 14, 15 and 17 into the dimensionless form of Eqs. 1 and 2, and collecting the terms of order ε^0 and ε leads to the zeroth-order equations,

$$\frac{\mathrm{d}J_\pm^{(0)}}{\mathrm{d}x} = 0, \quad J_\pm^{(0)} = -D_\pm^{\mathrm{ref}} e^{b_\pm j_\phi^{(0)}} \left(\frac{\mathrm{d}c_\pm^{(0)}}{\mathrm{d}x} + z_\pm c_\pm^{(0)} j_\phi^{(0)} \right),$$
$$-\frac{\mathrm{d}^2\phi^{(0)}}{\mathrm{d}x^2} = \frac{z_+ c_+^{(0)} + z_- c_-^{(0)}}{2\lambda_D^2}; \qquad [18]$$

and the first-order equations,

$$-\frac{\mathrm{d}}{\mathrm{d}x}\left(J_\pm^{(1)} + b_\pm J_\pm^{(0)} \frac{\mathrm{d}\phi^{(1)}}{\mathrm{d}x} \right) = (w + D_\pm^{\mathrm{ref}} k^2) c_\pm^{(1)}$$
$$+ D_\pm^{\mathrm{ref}} k^2 z_\pm c_\pm^{(0)} \phi^{(1)}, \qquad [19a]$$

$$-\frac{\mathrm{d}^2\phi^{(1)}}{\mathrm{d}x^2} + k^2\phi^{(1)} = \frac{z_+ c_+^{(1)} + z_- c_-^{(1)}}{2\lambda_D^2}, \qquad [19b]$$

$$J_\pm^{(1)} = -D_\pm^{\mathrm{ref}} e^{b_\pm j_\phi^{(0)}} \left(\frac{\mathrm{d}c_\pm^{(1)}}{\mathrm{d}x} + z_\pm c_\pm^{(1)} j_\phi^{(0)} + z_\pm c_\pm^{(0)} \frac{\mathrm{d}\phi^{(1)}}{\mathrm{d}x} \right). \qquad [19c]$$

It follows from Eq. 18 that $J_\pm^{(0)} = \mathrm{const}$. Hence, Eq. 19a is transformed into

$$-\frac{\mathrm{d}J_\pm^{(1)}}{\mathrm{d}x} - b_\pm J_\pm^{(0)} \frac{\mathrm{d}^2\phi^{(1)}}{\mathrm{d}x^2} = (w + D_\pm^{\mathrm{ref}} k^2) c_\pm^{(1)}$$
$$+ D_\pm^{\mathrm{ref}} k^2 z_\pm c_\pm^{(0)} \phi^{(1)}. \qquad [20]$$

The derivation of the boundary conditions on the evolving electrode surface $\Gamma(t)$, whose points are represented as $(y, h(y, t))^\top$, requires one to approximate $\phi(\mathbf{x} \in \Gamma, t)$, $c_\pm(\mathbf{x} \in \Gamma, t)$ and their gradients. That is accomplished by expanding these quantities in Taylor series around the base state $\Gamma^{(0)} = \{\mathbf{x} = (x, y)^\top : x = h^{(0)}, 0 \leqslant y \leqslant B/L\}$ such that

$$\phi(\mathbf{x} \in \Gamma, t) \approx \phi^{(0)}(h^{(0)}) + \hat{\varepsilon}\hat{\phi},$$
$$\hat{\phi}^{(1)} = \left(h^{(1)} \frac{\mathrm{d}\phi^{(0)}}{\mathrm{d}x} + \phi^{(1)} \right)_{x=h^{(0)}}; \qquad [21a]$$

$$c_\pm(\mathbf{x} \in \Gamma, t) \approx c_\pm^{(0)}(h^{(0)}) + \hat{\varepsilon}\hat{c}_\pm,$$
$$\hat{c}_\pm^{(1)} = \left(h^{(1)} \frac{\mathrm{d}c_\pm^{(0)}}{\mathrm{d}x} + c_\pm^{(1)} \right)_{x=h^{(0)}}; \qquad [21b]$$

and

$$\nabla\phi(\mathbf{x} \in \Gamma, t) \approx \mathbf{e}_x \left[\frac{\mathrm{d}\phi^{(0)}}{\mathrm{d}x}(h^{(0)}) \right.$$
$$\left. + \hat{\varepsilon}\left(h^{(1)} \frac{\mathrm{d}^2\phi^{(0)}}{\mathrm{d}x^2} + \frac{\mathrm{d}\phi^{(1)}}{\mathrm{d}x} \right)_{x=h^{(0)}} \right]$$
$$+ \mathbf{e}_y \hat{\varepsilon} ik\phi^{(1)}(h^{(0)}); \qquad [21c]$$

$$\nabla c_\pm(\mathbf{x} \in \Gamma, t) \approx \mathbf{e}_x \left[\frac{\mathrm{d}c_\pm^{(0)}}{\mathrm{d}x}(h^{(0)}) + \hat{\varepsilon}\left(h^{(1)} \frac{\mathrm{d}^2 c_\pm^{(0)}}{\mathrm{d}x^2} + \frac{\mathrm{d}c_\pm^{(1)}}{\mathrm{d}x} \right)_{x=h^{(0)}} \right]$$
$$+ \mathbf{e}_y \hat{\varepsilon} ik c_\pm^{(1)}(h^{(0)}). \qquad [21d]$$

The function $h^{(0)}(t)$ and the constant $h^{(1)}$ are first defined in Eqs. 12 and 13, respectively. It follows from Eq. 8 that first-order approximations of the unit normal vector $\mathbf{n} = \mathbf{n}^{(0)} + \mathcal{O}(\varepsilon^2)$ and the curvature are, respectively, $\kappa = \kappa^{(0)} + \hat{\varepsilon}\kappa^{(1)}$, with the components

$$\mathbf{n}^{(0)} = \begin{pmatrix} -1 \\ 0 \end{pmatrix}, \quad \kappa^{(0)} = 0,$$
$$\kappa^{(1)} = \frac{k^2}{2} h^{(1)}. \qquad [22]$$

Hence, a first-order approximation of the reaction rate R_{Li} in Eq. 12c, has the components $R_{Li}^{(0)}$ and $R_{Li}^{(0)}$ given by Eqs. 24c and 26c. The current density I is expanded to first order, $I = I^{(0)} + \hat{\varepsilon} I^{(1)}$, with $I^{(0)} = zR^{(0)}$ and $J^{(1)} = zR^{(1)}$.

The interface $h^{(0)}(t)$ is moving with velocity $U = \mathrm{d}h^{(0)}/\mathrm{d}t$. It follows from Eq. 9 that this velocity is given by $U = -\omega R_{Li}^{(0)}$. We introduce the moving coordinate system associated with the electrode-electrolyte interface, $(\xi \equiv x - Ut, y)$. Rewriting Eqs. 17–22 in this coordinate system yields the following zeroth- and first-order boundary-value problems (BVPs).

Base-state BVP.—The base-state dependent variables $c_\pm^{(0)}(\xi)$ and $\phi^{(0)}(\xi)$ satisfy the one-dimensional steady-state Poisson-Nernst-Planck equations:

$$\frac{\mathrm{d}J_\pm^{(0)}}{\mathrm{d}\xi} = 0, \qquad -\frac{\mathrm{d}^2\phi^{(0)}}{\mathrm{d}\xi^2} = \frac{z_+ c_+^{(0)} + z_- c_-^{(0)}}{2\lambda_D^2}, \qquad 0 < \xi < 1,$$
$$[23a]$$

where

$$J_\pm^{(0)} = -D_\pm^{\mathrm{ref}} e^{b_\pm j_\phi^{(0)}} \left(\frac{\mathrm{d}c_\pm^{(0)}}{\mathrm{d}\xi} + z_\pm j_\phi^{(0)} c_\pm^{(0)} \right),$$
$$j_\phi^{(0)} \equiv \frac{\mathrm{d}\phi^{(0)}}{\mathrm{d}\xi}. \qquad [23b]$$

Equation 23 are subject to the boundary conditions at the non-perturbed anode-surface, $\xi = 0$,

$$\frac{\mathrm{d}c_+^{(0)}}{\mathrm{d}\xi} = 0, \qquad -J_+^{(0)} = R_{Li}^{(0)}, \qquad \frac{\mathrm{d}c_-^{(0)}}{\mathrm{d}\xi} + z_- c_-^{(0)} j_\phi^{(0)} = 0; \quad [24a]$$

and at the outer surface of the electrolyte, $\xi = 1$,

$$\phi^{(0)}(1) = 0, \qquad c_+^{(0)}(1) = 1, \qquad c_-^{(0)}(1) = 1. \qquad \text{[24b]}$$

In 24a,

$$R_{Li}^{(0)} = -k_0 e^{-\alpha_{cat} z \eta_\alpha^{(0)}}(e^{z\eta_\alpha^{(0)}} - c_+^{(0)}/c_+^\Theta), \qquad \eta_\alpha^{(0)} = \phi_e - \phi^{(0)} - E^\Theta.$$
$$\text{[24c]}$$

Perturbed-state BVP.—The perturbed-state variables $c_\pm^{(1)}(\xi)$ and $\phi^{(1)}(\xi)$ satisfy the one-dimensional differential Eqs.

$$-\frac{dJ_\pm^{(1)}}{d\xi} - b_\pm J_\pm^{(0)} \frac{d^2\phi^{(1)}}{d\xi^2} = (w + D_\pm^{\text{ref}} k^2)c_\pm^{(1)} + D_\pm^{\text{ref}} k^2 z_\pm c_\pm^{(0)} \phi^{(1)},$$
$$\text{[25a]}$$

$$-\frac{d^2\phi^{(1)}}{d\xi^2} + k^2\phi^{(1)} = \frac{z_+ c_+^{(1)} + z_- c_-^{(1)}}{2\lambda_D^2}, \qquad \text{[25b]}$$

$$J_\pm^{(1)} = -D_\pm^{\text{ref}} e^{b_\pm j_\phi^{(0)}} \left(\frac{dc_\pm^{(1)}}{d\xi} + z_\pm c_\pm^{(1)} j_\phi^{(0)} + z_\pm c_\pm^{(0)} \frac{d\phi^{(1)}}{d\xi} \right). \qquad \text{[25c]}$$

Equation 25 are subject to the boundary conditions at $\xi = 0$,

$$wh^{(1)} = \omega c_0 R_{Li}^{(1)}, \qquad \frac{d\hat{c}_+^{(1)}}{d\xi} = 0,$$
$$\hat{J}_-^{(1)} = 0, \qquad -\hat{J}_+^{(1)} = R_{Li}^{(1)}, \qquad \text{[26a]}$$

and at $\xi = 1$,

$$\phi^{(1)}(1) = 0, \qquad c_+^{(1)}(1) = 0, \qquad c_-^{(1)}(1) = 0. \qquad \text{[26b]}$$

In these conditions, which are obtained as first-order approximations of Eqs. 3–10,

$$R_{Li}^{(1)} = k_0 e^{-\alpha_{cat} z \eta_\alpha^{(0)}} \left\{ \frac{\hat{c}_+^{(1)}}{c_+^\Theta} + \left[(1 - \alpha_{cat}) e^{z\eta_\alpha^{(0)}} + \alpha_{cat} \frac{c_+^{(0)}}{c_+^\Theta} \right] \right.$$
$$\left. \times (z\hat{\phi}^{(1)} - Cak^2 h^{(1)}) \right\}, \qquad \text{[26c]}$$

$$\hat{J}_\pm^{(1)} = -D_\pm^{\text{ref}} e^{b_\pm j_\phi^{(0)}} \left(\frac{d\hat{c}_\pm^{(1)}}{d\xi} + z_\pm c_\pm^{(1)} j_\phi^{(0)} + z_\pm c_\pm^{(0)} \frac{d\hat{\phi}^{(1)}}{d\xi} \right), \qquad \text{[26d]}$$

where

$$\hat{\phi}^{(1)} = h^{(1)} \frac{d\phi^{(0)}}{d\xi} + \phi^{(1)},$$

$$\hat{c}_\pm^{(1)} = h^{(1)} \frac{dc_\pm^{(0)}}{d\xi} + c_\pm^{(1)}. \qquad \text{[26e]}$$

Perturbed-state BVP for anisotropic constant diffusion.— Another problem of practical significance involves anisotropic electrolytes in which the diffusion coefficient tensor in Eq. 11 is replaced with Eq. 16. The procedure used above yields the base-state dynamics described by Eqs. 23a and 24 with $D_\pm^{\text{ref}} = D_{xx}^\pm$ and $b_\pm = 0$. It also leads to the perturbed-state equations

$$\frac{dJ_\pm^{(1)}}{d\xi} + w c_\pm^{(1)} + k^2 D_{yy}^\pm (c_\pm^{(1)} + z_\pm c_\pm^{(0)} \phi^{(1)}) = 0, \qquad \text{[27]}$$

$$-\frac{d^2\phi^{(1)}}{d\xi^2} + k^2\phi^{(1)} = \frac{z_+ c_+^{(1)} + z_- c_-^{(1)}}{2\lambda_D^2},$$
$$J_\pm^{(1)} = -D_{xx}^\pm \left[\frac{dc_\pm^{(1)}}{d\xi} + z_\pm \left(c_\pm^{(1)} j_\phi^{(0)} + c_\pm^0 \frac{d\phi^{(1)}}{d\xi} \right) \right] \qquad \text{[28]}$$

and the boundary conditions at $\xi = 0$

$$h^{(1)} \frac{dJ_-^{(0)}}{d\xi} + J_-^{(1)} = 0, \qquad h^{(1)} \frac{dJ_+^{(0)}}{d\xi} + J_+^{(1)} = -R_{Li}^{(1)},$$

$$\frac{d\hat{c}_+^{(1)}}{d\xi} = 0, \qquad wh^{(1)} = \omega c_0 R_{Li}^{(1)}; \qquad \text{[29]}$$

and at $\xi = 1$

$$\phi^{(1)} = 0, \qquad c_\pm^{(1)} = 0. \qquad \text{[30]}$$

Here, $J_\pm^{(0)}$ and $\hat{c}_+^{(1)}$ are defined by Eq. 23b with $D_\pm^{\text{ref}} = D_{xx}^\pm$ and $b_\pm = 0$ and by Eq. 26e, respectively.

ORCID

Daniel M. Tartakovsky https://orcid.org/0000-0001-9019-8935

References

1. O. Crowther and A. C. West, "Effect of electrolyte composition on lithium dendrite growth." *J. Electrochem. Soc.*, **155**, A806 (2008).
2. A. Aryanfar, D. Brooks, B. V. Merinov, W. A. Goddard III, A. J. Colussi, and M. R. Hoffmann, "Dynamics of lithium dendrite growth and inhibition: pulse charging experiments and Monte Carlo calculations." *J. Phys. Chem. Lett.*, **5**, 1721 (2014).
3. Q. Chen, K. Geng, and K. Sieradzki, "Prospects for dendrite-free cycling of Li metal batteries." *J. Electrochem. Soc.*, **162**, A2004 (2015).
4. P. Bai, J. Li, F. R. Brushett, and M. Z. Bazant, "Transition of lithium growth mechanisms in liquid electrolytes." *Energy & Environmental Science*, **9**, 3221 (2016).
5. A. Riaz and H. A. Tchelepi, "Linear stability analysis of immiscible two-phase flow in porous media with capillary dispersion and density variation." *Phys. Fluids*, **16**, 4727 (2004).
6. H. Zhong, M. N. Shneider, X. Mao, and Y. Ju, "Dynamics and chemical mode analysis of plasma thermal-chemical instability." *Plasma Sources Sci. Technol.*, **30**, 3 (2021).
7. L. G. Sundström and F. H. Bark, "On morphological instability during electrodeposition with a stagnant binary electrolyte." *Electrochimica Acta*, **2**, 7 (1995).
8. J. Elezgaray, C. Léger, and F. Argoul, "Linear stability analysis of unsteady galvanostatic electrodeposition in the two-dimensional diffusion-limited regime." *J. Electrochem. Soc.*, **145**, 2016 (1998).
9. M. D. Tikekar, L. A. Archer, and D. L. Koch, "Stability analysis of electrodeposition across a structured electrolyte with immobilized anions." *J. Electrochem. Soc.*, **161**, A847 (2014).
10. E. Khoo, H. Zhao, and M. Z. Bazant, "Linear stability analysis of transient electrodeposition in charged porous media: suppression of dendritic growth by surface conduction." *J. Electrochem. Soc.*, **166**, A2280 (2019).
11. A. Verma, H. Kawakami, H. Wada, A. Hirowatari, N. Ikeda, Y. Mizuno, T. Kotaka, K. Aotani, Y. Tabuchi, and P. P. Mukherjee, "Microstructure and pressure-driven electrodeposition stability in solid-state batteries." *Cell Reports Physical Science*, **2**, 100301 (2021).
12. M. D. Tikekar, L. A. Archer, and D. L. Koch, "Stabilizing electrodeposition in elastic solid electrolytes containing immobilized anions." *Sci. Adv.*, **2**, 7 (2016).
13. M. D. Tikekar, G. Li, L. A. Archer, and D. L. Koch, "Electroconvection and morphological instabilities in potentiostatic electrodeposition across liquid electrolytes with polymer additives." *J. Electrochem. Soc.*, **165**, A3697 (2018).
14. T. Gao, G. Liu, and W. Lu, "A theory that couples electrochemistry and thin film piezoelectricity with stability analysis for electrodeposition." *Journal of the Mechanics and Physics of Solids*, **162**, 104827 (2022).
15. A. Ganesh, D. S. Pillai, and R. Narayanan, "Effect of low-frequency AC forcing on the morphological instability arising in electrodeposition." *Journal of Engineering Mathematics*, **132**, 1 (2022).
16. T. J. Rademaker, G. R. A. Akkermans, D. L. Danilov, and P. H. L. Notten, "On the deviation of electro-neutrality in Li-ion battery electrolytes." *J. Electrochem. Soc.*, **161**, E3365 (2014).
17. X. Wang, M. Chen, S. Li, C. Zhao, W. Zhang, Z. Shen, Y. He, G. Feng, and Y. Lu, "Inhibiting dendrite growth via regulating the electrified interface for fast-charging lithium metal anode." *ACS Central Science*, **7**, 2029 (2021).
18. J. Zheng, M. H. Engelhard, D. Mei, S. Jiao, B. J. Polzin, J.-G. Zhang, and W. Xu, "Electrolyte additive enabled fast charging and stable cycling lithium metal batteries." *Nat. Energy*, **2**, 1 (2017).

19. C. P. Nielsen and H. Bruus, "Morphological instability during steady electro-deposition at overlimiting currents." *Physical Review E*, **92**, 52310 (2015).

20. J.-N. Chazalviel, "Electrochemical aspects of the generation of ramified metallic electrodeposits." *Phys. Rev. A*, **42**, 15 (1990).

21. C. L. Druzgalski, M. B. Andersen, and A. Mani, "Direct numerical simulation of electroconvective instability and hydrodynamic chaos near an ion-selective sur-face." *Phys. Fluids*, **25**, 110804 (2013).

22. M. Rosso, T. Gobron, C. Brissot, J. N. Chazalviel, and S. Lascaud, "Onset of dendritic growth in lithium/polymer cells." *Journal of Power Sources*, **97–98**, 804 (2001).

23. J. Tan, A. M. Tartakovsky, K. Ferris, and E. M. Ryan, "Investigating the effects of anisotropic mass transport on dendrite growth in high energy density lithium batteries." *J. Electrochem. Soc.*, **163**, A318 (2016).

24. S. Murad, "The role of external electric fields in enhancing ion mobility, drift velocity, and drift-diffusion rates in aqueous electrolyte solutions." *The Journal of Chemical Physics*, **134**, 114504 (2011).

25. V. Ponce, D. E. Galvez-Aranda, and J. M. Seminario, "Analysis of a Li-ion nanobattery with graphite anode using molecular dynamics simulations." *Journal of Physical Chemistry C*, **121**, 12959 (2017).

26. B. Ravikumar, M. Mynam, and B. Rai, "Molecular dynamics investigation of electric field altered behavior of lithium ion battery electrolytes." *Journal of Molecular Liquids*, **300**, 112252 (2020).

27. M. Liu, P. J. Chimtali, X. B. Huang, and R. B. Zhang, "Structures and dynamic properties of the LiPF6 electrolytic solution under electric fields–a theoretical study." *Phys. Chem. Chem. Phys.*, **21**, 13186 (2019).

28. L. O. Valøen and J. N. Reimers, "Transport properties of LiPF6-based Li-ion battery electrolytes." *J. Electrochem. Soc.*, **152**, A882 (2005).

29. S. Stewart and J. Newman, "Measuring the salt activity coefficient in lithium-battery electrolytes." *J. Electrochem. Soc.*, **155**, A458 (2008).

30. T. Hou, G. Yang, N. N. Rajput, J. Self, S. W. Park, J. Nanda, and K. A. Persson, "The influence of FEC on the solvation structure and reduction reaction of LiPF6/EC electrolytes and its implication for solid electrolyte interphase formation." *Nano Energy*, **64**, 103881 (2019).

31. R. John, *CRC Handbook of Chemistry and Physics* (CRC Press, Boca Raton, FL) (2021) 102nd ed., (Internet Version 2021).

32. R. Naejus, D. Lemordant, R. Coudert, and P. Willmann, "Excess thermodynamic properties of binary mixtures containing linear or cyclic carbonates as solvents at the temperatures 298.15 K and 315.15 K." *The Journal of Chemical Thermodynamics*, **29**, 15031515 (1997).

33. CODATA Value: vacuum electric permittivity. https://physics.nist.gov/cgi-bin/cuu/Value?ep0.

34. S. Xu, K.-H. Chen, N. P. Dasgupta, J. B. Siegel, and A. G. Stefanopoulou, "Evolution of dead lithium growth in lithium metal batteries: experimentally validated model of the apparent capacity loss." *J. Electrochem. Soc.*, **166**, A3456 (2019).

35. C. T. Tan and G. M. Homsy, "Stability of miscible displacements in porous media: rectilinear flow." *Phys. Fluids*, **29**, 3549 (1986).

36. Y. C. Yortsos and M. Zeybek, "Dispersion driven instability in miscible displace-ment in porous media." *Phys. Fluids*, **31**, 3511 (1988).

37. A. Riaz and H. A. Tchelepi, "Influence of relative permeability on the stability characteristics of immiscible flow in porous media." *Transport in Porous Media*, **64**, 315 (2006).

38. A. Riaz and H. A. Tchelepi, "Stability of two-phase vertical flow in homogeneous porous media." *Phys. Fluids*, **19**, 72103 (2007).

39. M. Haataja, D. J. Srolovitz, and A. B. Bocarsly, "Morphological stability during electrodeposition: I. Steady states and stability analysis." *J. Electrochem. Soc.*, **150**, C699 (2003).

40. M. Haataja, D. J. Srolovitz, and A. B. Bocarsly, "Morphological stability during electrodeposition: II. Additive effects." *J. Electrochem. Soc.*, **150**, C708 (2003).

41. L. Chen, H. W. Zhang, L. Y. Liang, Z. Liu, Y. Qi, P. Lu, J. Chen, and L.-Q. Chen, "Modulation of dendritic patterns during electrodeposition: a nonlinear phase-field model." *Journal of Power Sources*, **300**, 376 (2015).

42. Z. Hong and V. Viswanathan, "Phase-field simulations of lithium dendrite growth with open-source software." *ACS Energy Lett.*, **3**, 1737 (2018).

43. X. Fan and C. Wang, "High-voltage liquid electrolytes for Li batteries: progress and perspectives." *Chem. Soc. Rev.*, **50**, 10486 (2021).

44. W. Li and D. M. Tartakovsky, "Effective representation of active material and carbon binder in porous electrodes." *J. Electrochem. Soc.*, **169**, 040556 (2022).

45. K. Xu and A. Von Wald Cresce, "Li-solvation/desolvation dictates interphasial processes on graphitic anode in Li ion cells." *J. Mater. Res.*, **27**, 2327 (2012).

46. Y. Kondo, T. Abe, and Y. Yamada, "Kinetics of interfacial ion transfer in lithium-ion batteries: mechanism understanding and improvement strategies." *ACS Appl. Mater. Interfaces*, **14**, 22706 (2022).